ACS OMEGA

http://pubs.acs.org/journal/acsodf

Article

# Estimations of Fe−$N_2$ Intrinsic Interaction Energies of Iron−Sulfur/Nitrogen−Carbon Sites: A Deeper Bonding Insight by EDA-NOCV Analysis of a Model Complex of the Nitrogenase Cofactor

Sai Manoj N. V. T. Gorantla and Kartik Chandra Mondal*

Cite This: *ACS Omega* 2021, 6, 33932−33942

Read Online

ACCESS | Metrics & More | Article Recommendations | Supporting Information

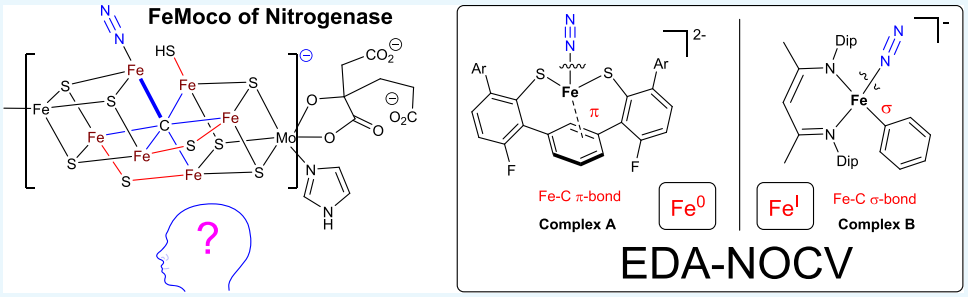


**ABSTRACT:** The $MoFe_7S_9C^{1-}$ unit of the nitrogenase cofactor (FeMoco) attracts chemists and biochemists due to its unusual ability to bind aerial dinitrogen ($N_2$) at ambient condition and catalytically convert it into ammonia ($NH_3$). The mode of $N_2$ binding and its reaction pathways are yet not clear. An important conclusion has been made based on the very recent synthesis and isolation of model Fe(I/0)-complexes with sulfur-donor ligands under the cleavage of one Fe−S bond followed by binding of $N_2$ at the Fe(0) center. These complexes are structurally relevant to the nitrogenase cofactor ($MoFe_7S_9C^{1-}$). Herein, we report the EDA-NOCV analyses and NICS calculations of the dinitrogen-bonded dianionic complex $Fe^0$−$N_2$ (**1**) (having a $C_{Ar}$ ← Fe $\pi$-bond) and monoanionic complex $Fe^I$−$N_2$ (**2**) (having a $C_{Ar}$−Fe $\sigma$-bond) to provide a deeper insight into the Fe−$N_2$ interacting orbitals and corresponding pairwise interaction energies (EDA-NOCV = energy decomposition analysis coupled with natural orbital for chemical valence; NICS = nucleus-independent chemical shifts). The orbital interaction in the Fe−$N_2$ bond is significantly larger than Coulombic interactions, with major pairwise contributions coming from d(Fe) orbitals to the empty $\pi^*$ orbitals of $N_2$ (three Fe → $N_2$). $\Delta E_{int}$ values are in the range of −61 to −77 kcal $mol^{-1}$. Very interestingly, NICS calculations have been carried out for the fragments before and after binding of the $N_2$ molecule. The computed $\sigma$- and $\pi$-aromaticity values are attributed to the position of the Fe atoms, oxidation states of Fe centers, and Fe−C bond lengths of these two complexes.

## INTRODUCTION

Dinitrogen ($N_2$) binding and catalytic reductive protonation leading to the formation of ammonia ($NH_3$) are some of the most important biochemical natural processes on the planet.[1−3] The reduced forms of $N_2$ (bio-organic molecules such as amino acid, peptide, nucleotide and nucleic acid etc.) are the parts of different forms that are the building blocks of the living organism, plants, and animals.[4] However, most of the living species on the earth cannot directly utilize the aerial $N_2$ molecule although it is 78% of atmosphere of our planet. This is due to the kinetic inertness of molecular dinitrogen. The detailed bonding analysis (energy decomposition analysis coupled with natural orbital for chemical valence (EDA-NOCV))[5] of $N_2$ suggests that the Wiberg bond order of $N_2$ is little above three (3.03), possessing two $\pi$-bonds and one $\sigma$-bond with overall 70% covalent orbital ($\Delta E_{orb}$) and 30% electrostatic ($\Delta E_{elstat}$) contributions. The $\sigma$ and $\pi$ contributions are 65.6 and 34.4%, respectively. The very short N−N distance of 1.102 Å contributes to a high Pauling repulsion ($\Delta E_{Pauli}$) energy.[5] Molecular $N_2$ (:N≡N:) contains two low-lying pairs of electrons ($\sigma/\sigma^*$) in $2\sigma_g^+/2\sigma_u^+$ that are not efficient for $\sigma$-donation, while its doubly degenerate filled $\pi$-orbitals ($1\pi_u$) (HOMO−1; Scheme 1, top) and doubly occupied $3\sigma_g^+$ (HOMO) orbital are higher in energy and are available for bonding with acceptors in certain circumstances.[6] The LUMO and LUMO+1 are the doubly degenerate $\pi^*$ ($1\pi_g$) orbital and $\sigma^*$ orbital ($3\sigma_u^+$) of $N_2$,[5] respectively, which are available for $\pi$-backdonations from metal atoms (Scheme 1) to accept electron densities, leading to the crucial elongation/activation of the N−N bond.

Received: September 21, 2021
Accepted: November 10, 2021
Published: December 2, 2021

**Scheme 1. (Top) Shape of the MO of Bonding and Antibonding Orbitals and (Bottom) End-On Orbital Interactions between Metal-Atom (M) and the $N_2$ Molecule**

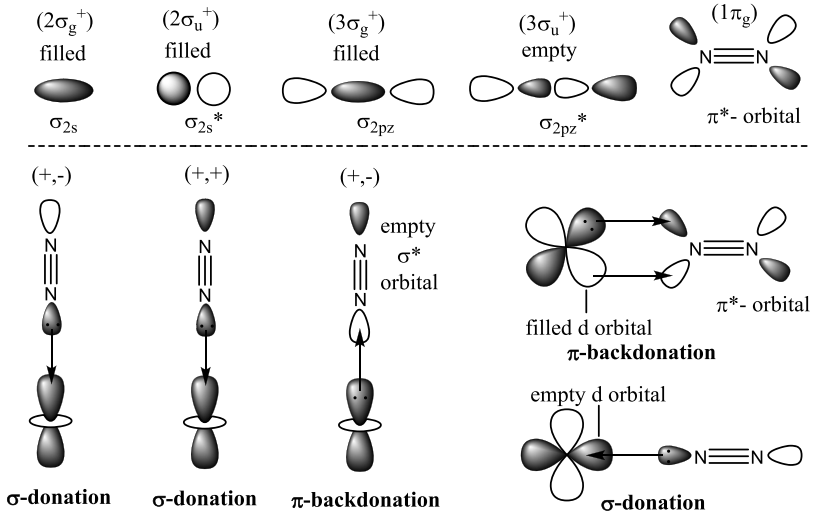


**Scheme 2. Speculated $N_2$ Binding by the Fe Center of the FeMoCo Cluster of the Nitrogenase Enzyme (Top) and Previously Reported Model Complex[26] under Reduced State with Cleavage of the Fe−S Bond**

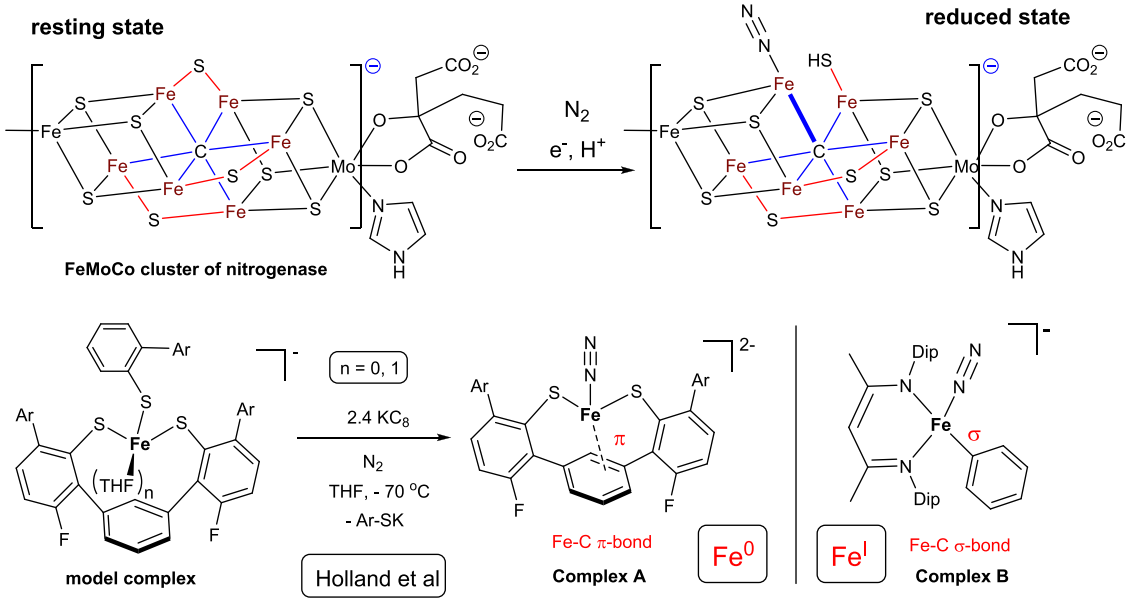


Diazotrophs are bacteria and archaea that can bind areal $N_2$ and transform it into a more stable reduced form such as ammonia. They live in the soil. A family of plants, called legume, whose roots are infected with nitrogen-fixing bacteria such as azotobacter start living in the plant's root. This bacterium provides nitrogen products to legume pants by utilizing direct $N_2$ from air. The active enzyme of azotobacter is nitrogenase, which possesses a monoanionic inorganic cluster $[Mo(+3)Fe(+2.5)_4Fe(+3)_2Fe(+2)S(-2)_9C(-4); (MoFe_7S_9C)^{1-}]$.[7] This coordination cluster is protected from undergoing aerial oxidation by the protein part of this enzyme. Two Fe−S/Fe−Mo−S hetero-cubane units ($Fe_4S_3$ and $MoFe_3S_3$) are connected by a hexacoordinate lighter element (carbon) and three $\mu_3$-S bridges to form the monoanionic inorganic core $MoFe_7S_9C^{1-}$ having nine bridging anions $S^{2-}$ and one $\mu_6$-$C^{4-}$ anion. $MoFe_7S_9C^{1-}$ (Scheme 2; top right) has a ground-state spin $S = 3/2$ in the resting state.[1,2] Kinetic studies have shown that it does not bind to molecular $N_2$ in the resting state. Rather it binds with $N_2$ under reduced form (Scheme 2, top right) when another $Fe_4S_4$ unit (P-cluster) transfers the required number of electrons.[1,2] However, the modes of $N_2$ binding and the reaction paths of $N_2$ reduction by nitrogenase are still not clear. Several model Fe complexes have been reported over the past two decades to shed light on the structure, electronic properties, and reactivity of the nitrogenase enzyme.[7−27] Based on the experimental evidences, it has been concluded that one of the six Fe centers that are bonded to the central C-atom is expected to bind with $N_2$ under reduced state with the cleavage of one Fe−S bond. The coordination geometry of that particular Fe center is speculated to be four, with an $S_2CN$ coordination environment (Scheme 2).[26] Recently, the group of Holland has designed an $S_2(\eta^2\text{-}C_{Ar})$-donor ligand (Scheme 2), which has been further utilized for the syntheses of Fe(II/I/0) complexes. Holland et al. experimentally observed that under reduced condition, one Fe−S−Ar of the modelled complex is broken with the


https://doi.org/10.1021/acsomega.1c05238
ACS Omega 2021, 6, 33932−33942

**Scheme 3. Axial (Left; Fe−C Bond Elongation) and Equatorial (Right) $N_2$ Bonding at the Fe Center of Nitrogenase**

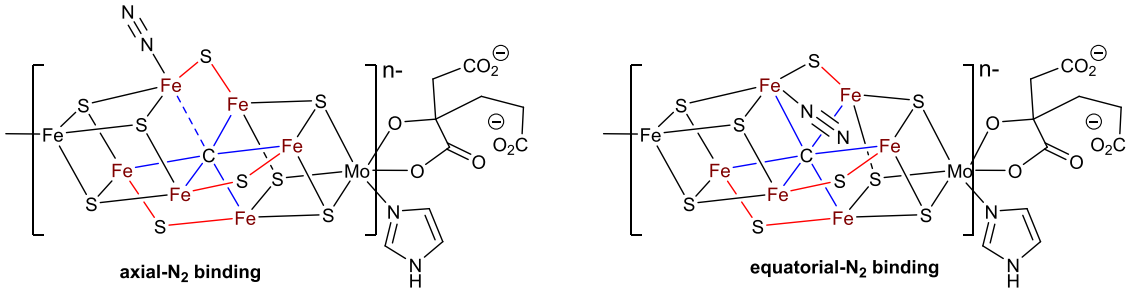


**Scheme 4. Simplified Structures of Complexes 1 and 2 that Have Been Modelled**

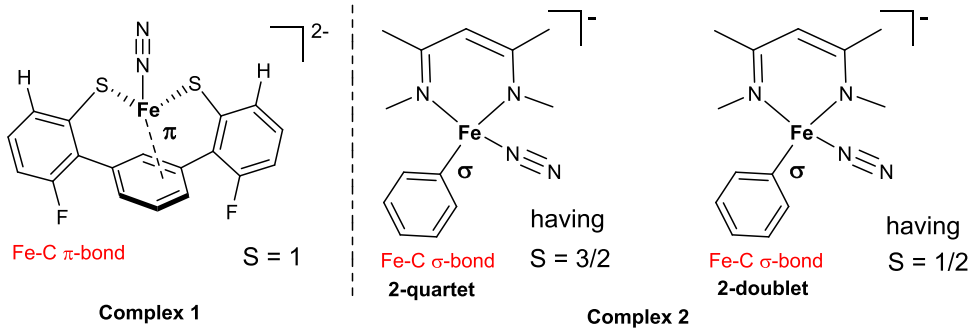


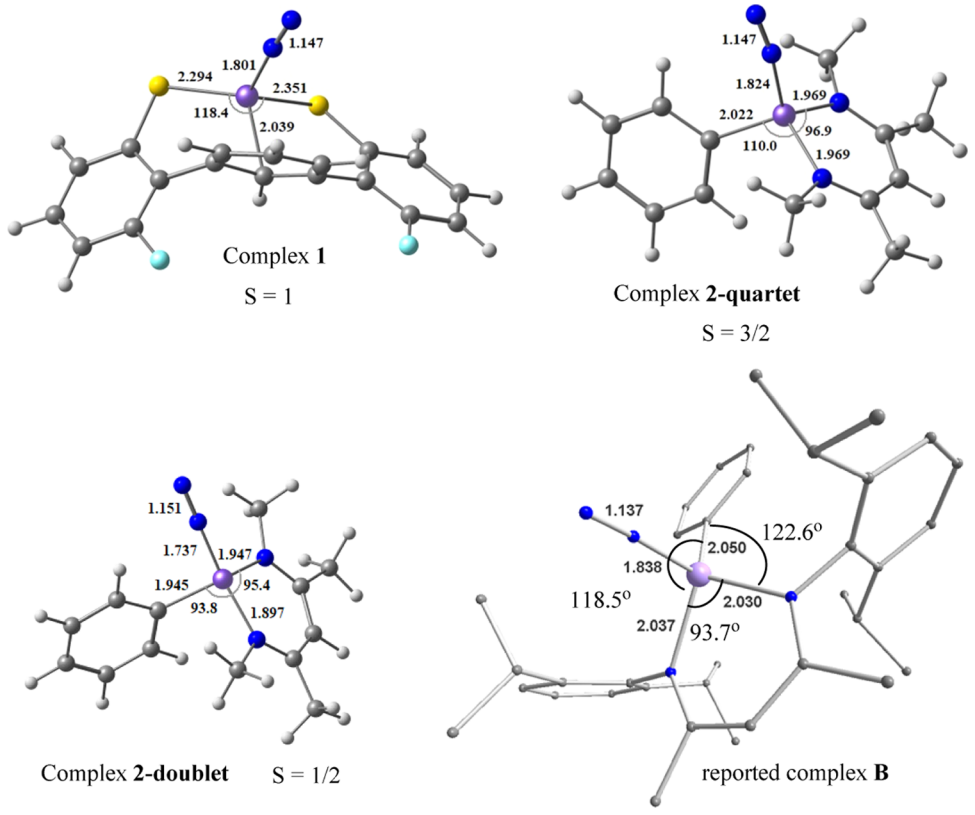


**Figure 1.** Optimized geometries of complexes **1**, **2** at BP86-D3(BJ)/Def2TZVPP level of theory and of previously reported complex **B**.

formation of the Fe−$N_2$ bond (Scheme 1).[26] Very recently they have suggested[26] that cleavage of the Fe−S bond is more likely rather than elongation of the Fe−$C_{central}$ bond or dissociation of the Fe−$C_{central}$ bond of the $MoFe_7S_9C$ cluster of the nitrogenase enzyme under reduced condition during binding of $N_2$ (Schemes 2 and 3).

Syntheses of several modelled complexes have been reported, having M−$N_2$ bonds for the purpose of dinitrogen reduction to ammonia.[8−26] The importance of activation of the $N_2$ bond has been emphasized, and the extent of backdonation has been correlated with $\upsilon_{N-N}$ IR stretching frequency. However, there is no report of any theoretical study on



https://doi.org/10.1021/acsomega.1c05238
ACS Omega 2021, 6, 33932−33942

estimation of the Fe−$N_2$ interaction energy for efficient binding of the $N_2$ molecule with the Fe center that could rationalize the syntheses and characterizations of this class of complexes.

Herein, we report on the DFT, NBO, QTAIM, NICS calculations, and, most importantly, EDA-NOCV analysis of previously reported dinitrogen-bonded $Fe^0$−$N_2$ (**1**) and $Fe^{+1}$−$N_2$ (**2**) complexes[26,27] to give a deeper insight into the nature of Fe−$N_2$ bonds and corresponding pairwise interaction energies. Interestingly, nucleus-independent chemical shift (NICS) calculations even gave a deeper insight into the extent of Fe → $C_{Ar}$ backdonation before and other binding with the $N_2$ molecule.

## RESULTS AND DISCUSSION

Holland and co-workers have isolated and crystallographically characterized $N_2$-bonded Fe complexes catering to two different applications:[26,27] dianionic dithiolate Fe−$N_2$ complex, designed to mimic and explain the $N_2$ binding of the nitrogenase enzyme,[26] and monoanionic L-Fe($N_2$)(Ph) [L = $\beta$-diketiminate] complex, as an intermediate in the activation of benzene and $N_2$ leading to the formation of aniline derivatives,[27] which we designate as complexes **A** and **B**, respectively (Schemes 2 and 4). The Fe center of **A** is coordinated by two sulfur and two carbon atoms of the $\eta^2$-aryl ring, whereas the Fe center of complex **B** is coordinated to two nitrogen atoms of $\beta$-diketiminate and one carbon atom of the phenyl group. Besides, the Fe atom of complex **A** interacts with the $\pi$ cloud of the aromatic carbon ring, while in complex **B** the Fe−C interaction is mostly a $\sigma$ type (Scheme 2). Despite their structural differences, the precursors of both complexes **A** and **B** bind with $N_2$ only under the reduced condition at low temperatures to produce **A**−**B**,[26,27] which is similar to the FeMoco cofactor of the nitrogenase enzyme.[26] However, complex **A** deviates from the nitrogenase enzyme in the Fe−C interaction (Fe···$C_2$(Ar); Scheme 4), where it is an $\sigma$-type bond (complex **B**, Fe−Ph; Scheme 4 right) in the latter and a $\pi$ type in the former (**A**). Both **A** and **B** show a pseudotetrahedral geometry at the iron site after binding to $N_2$. While the Fe−N bond distances are 1.790−1.839 Å, the N−N bond lengths of pseudoterminally bonded $N_2$ are 1.131−1.136 Å in the reported complexes **A** and **B**, respectively. Though these two complexes have been intended for different applications, the common theme they share is dinitrogen binding. Intrigued by this, we have modelled and optimized simplified versions of the reported complexes **A** and **B**, which we designate as complexes **1** and **2** (Scheme 4), respectively, to shed some light on the strength of $N_2$ binding to the Fe centers. We have optimized complex **1** in both singlet and triplet electronic states, while complex **2** was reported in the electronic quartet state and also in doublet state, in both the gas phase and THF at BP86-D3(BJ)/Def2TZVPP level (Scheme 4, Figure 1). The details of the computational methods are provided in the Supporting Information. The calculations suggest the energy of solvation as 127.4 (**1**) and 39.6 (**2**) kcal $mol^{-1}$; the geometrical parameters of the gas phase and THF optimized complexes are very close in both gas phase and solution. Herein, we report the geometrical parameters of the gas phase optimized structures. Complex **1** is comparatively more stable in the triplet state by 7.35 kcal $mol^{-1}$ in the gas phase and 6.93 kcal $mol^{-1}$ in THF solution. The authors have experimentally and theoretically proven the preference for the triplet state geometry over the singlet state in the reported complex **A**. However, in the case of complex **2**, calculations suggest that doublet state is more stable than the quartet state, by 6.4 kcal $mol^{-1}$ in the gas phase and 6.91 kcal $mol^{-1}$ in THF. Although the energy difference between the doublet and quartet states of complex **2** is small, we assume that it can exist in both states under experimental conditions. The coordinated sulfur atoms of complex **1** are at a distance of 2.294−2.351 Å from the Fe center with an S−Fe−S bond angle of 118.4°, while the coordinated carbon atom of the aromatic ring is at a distance of 2.039 (**1**) Å, which is very close to the experimental values (2.037 (**1**), 2.049 (**2**) Å) of original complexes **A**−**B**.[26,27] The optimized values correlate well with the reported Fe−S (2.320(16)−2.355(16) Å) and Fe−C (2.037(5) (**1**) Å) distances and S−Fe−S bond angle of 114.3° (**A**)/118.4° (**1**) (Figure 1). The Fe−C distances of **A** are 2.037 and 2.24 Å, which are close to those of **1** (2.05, 2.08 Å). The difference in the second Fe−C bond length can be attributed to the steric hindrance in **A**.[26]

The Fe(I) center ($3d^7$) of complex **2** has adopted a slightly distorted tetrahedral geometry. The deviation from perfect tetrahedral geometry can lift the degeneracy of the $t_{2g}$ level of the Fe(I) ion. Hence, **2** has been optimized in both quartet ($S$ = 3/2; **2-quartet**) and doublet ($S$ = 1/2; **2-doublet**). The coordinated nitrogen atoms of the ligand of **2-quartet** (Scheme 2, Figure 1) are equidistant (1.969 Å) from the Fe center, with the N−Fe−N bond angle of 96.9°. The Fe−$C_{Ph}$ bond distance of **2-quartet** is 2.022 Å. The optimized values concur well with those of the experimentally reported Fe−N (2.036 Å) and Fe−C (2.049 Å) bond lengths and the N−Fe−N bond angle of 93.7° of **B**.[27] The slight widening of the S−Fe−S and N−Fe−N bond angles in complexes **1** and **2-quatret** from the reported bond angles is owing to the presence of less bulky substituents, which reduces the steric repulsion (Figure 1). The structures of **1**, **2-quartet**, and **B** with selected bond parameters are given in Figure 1. The comparison between the bond parameters **2-quartet** and **2-doublet** clearly suggests that the spin ground state of **B** is most likely 3/2 (quartet). The Fe−$N_{N2}$ (1.838 Å, **B**) bond length is significantly farther from that of **2-doublet** (1.737 Å), but rather closer to **2-quartet** (1.824 Å). Other Fe−$N_L$ bond distances of **B** are little over 2 Å. The corresponding bond parameters of **2-doublet** are significantly shorter than those of **B**/**2-quartet**. The bulky substitution (like Dip-group = 2,6-disiopropylphenyl) on two N atoms of the $\beta$-diketiminate ligand (L) must have exerted a significant amount of steric effect/distortion, leading to a quartet as the ground state of **2**. Structural optimization with smaller substitutions (Me-group) at the BP86-D3(BJ)/Def2TZVPP level of theory favors the doublet state (**2-doublet**) over the quartet state (**2-quartet**) of **2**.

The Fe−$N_2$ bond length of complex **1** is slightly shorter (1.801 Å) than that of complex **2** (1.824 Å). However, the N−N bond lengths of coordinated $N_2$ in both complexes **1** and **2** are similar (1.147 Å) and are slightly elongated compared to the N≡N bond length of free $N_2$ (1.102 Å), suggesting strong Fe → $N_2$ backdonation. The Fe−$N_2$ bond dissociation energies [(L)Fe−$N_2$ → (L)Fe + $N_2$] of **1** and **2** are slightly endothermic both in the gas phase (20.9 (**1**), 15.8 (**2**) kcal $mol^{-1}$) and in THF (17.1 (**1**), 16.1 (**2**) kcal $mol^{-1}$). The energy of dissociation in the gas phase is 33.2 and 27.0 kcal $mol^{-1}$ for **1** and **2**, respectively.



https://doi.org/10.1021/acsomega.1c05238
ACS Omega 2021, 6, 33932−33942

## COMPUTATIONAL METHOD

The EDA-NOCV method[28−37] is more appropriate in explaining the nature of the bond as one of the major strengths of the method is its ability to provide the best bonding model to represent the bonding situation in the equilibrium geometry.[35,36] However, the EDA-NOCV analysis of paramagnetic species is quite challenging as the main problem of EDA-NOCV calculations of paramagnetic species is to reflect physically meaningful orbital occupations in both possible situations: the bound complex and the isolated fragments. Especially in complexes involving 3d metal ions, it is a challenge to identify the d-orbitals with unpaired electrons to achieve meaningful orbital occupations in the isolated fragments, and thus in the bound complex, for accurate EDA-NOCV analysis.[37] The EDA-NOCV method[28−37] decomposes the intrinsic interaction energy ($\Delta E_{int}$) between two fragments into four energy components as given below

$$\Delta E_{int} = \Delta E_{elstat} + \Delta E_{Pauli} + \Delta E_{orb} + \Delta E_{disp} \quad (1)$$

where the electrostatic term ($\Delta E_{elstat}$) arises from the interpenetrating charges of the nuclei of the two fragments that attract the electron cloud of the opposite fragment, and the orbital term ($\Delta E_{orb}$) comes from the mixing and relaxation of the orbitals, charge transfer, and polarization between the isolated fragments. The dispersion energy ($\Delta E_{disp}$) arises from the noncovalent interactions, and, in particular, weak London forces between the two interacting fragments. The above-mentioned terms represent attractive forces; the Pauli term ($\Delta E_{Pauli}$) arises due to the repulsion between the same electron spins of the two fragments when sharing the same bonding space. The corresponding deformation electron densities are represented by the direction of the charge flow red → blue.[36] The $N_2$ has been considered in singlet, and ligand-Fe is either in $S$ = 1 or in 1/2 or 3/2 spin state for our EDA-NOCV fragmentations and analyses.[37]

We have employed charge and energy density methods like natural bond orbital (NBO), quantum theory of atoms in molecules (QTAIM), and energy decomposition analysis coupled with natural orbitals for chemical valence (EDA-NOCV) methods to study the nature of the Fe−$N_2$ bond. The natural charge distribution of the dianionic dithiolate-Fe complex, a precursor of complex **1**, shows the concentration of charge on the sulfur atoms and faint positive charge on the Fe center. Upon binding to $N_2$, the charge gets depleted on the sulfur atoms, and rather charge concentration can be observed on the Fe center and the otherwise neutral $N_2$ (Table 1). This indicates the direction of charge flow $(C_{Ar})(S_2)$ → Fe → $N_2$. On the contrary, for monoanionic $[(NacNac)(C_6H_5)]$Fe, the precursor of complex **2** shows a positive charge on the Fe center and a negative charge on the ligand nitrogen atoms. However, after binding to $N_2$, the shift of charge is much more akin to complex **1** and the charge flows in the direction $(C_{Ph})(N_2)_L$ → Fe → $N_2$. The NBO calculation suggests a Wiberg bond index of 0.96, 0.85 for Fe−N bond and 2.48 for N−N bond in complex **1** and **2**, respectively.[26] The Fe−N and N−N bond orders are consistent with the Fe−N and N−N bond lengths in both the complexes. The decrease in N−N bond order (BO) of $N_2$ in complexes **1** and **2** compared to that of free $N_2$ (BO = 3.03) indicates the weakening of the N−N bond after complexation with metal, which is crucial for the activation of $N_2$. The $\alpha$-SOMO and $\alpha$-SOMO−1 of complex **1** represent the two unpaired electrons residing in $d_{z^2}$ and $d_{x^2y^2}$ of the triplet state (Figure S2), whereas $\alpha$-SOMO, $\alpha$-SOMO−1, and $\alpha$-SOMO−2 of complex **2** represent the three unpaired electrons residing in $d_{xz}$, $d_{z^2}$, and $d_{x^2y^2}$ of the quartet state (Figure S3). The unpaired electrons show some interaction with the p orbitals of $N_2$. The remaining d-orbitals of both complexes **1** and **2** represent $\pi$-interactions with the p orbitals of the dinitrogen.

**Table 1. Partial Charges on Fe, $N_2$, and $S_2$ Atoms of Complexes 1, 2-quartet and Their Precursors at the BP86/Def2-TZVPP Level of Theory**

| molecule | qFe | q$N_2$ | q$S_2$/$N_2$ | $C_{Ph}$ |
|---|---|---|---|---|
| complex **1** | −0.158 | −0.24 | −0.194 | −0.271 |
| $[S_2Fe]^{2-}$ | 0.016 | | −0.350 | −0.315 |
| complex **2-quartet** | +0.340 | −0.26 | −0.939 | −0.256 |
| $[(NacNac)C_6H_5)Fe]^-$ | +0.477 | | −1.07 | −0.372 |

The AIM analysis shows solid paths (Figure S4) indicating the chemical bond between the Fe and N atoms. The electron density $\rho(r)$ at the bond critical point (BCP) reflects the type of interaction and in turn the strength of the bond. The considerable electron densities of 0.132 and 0.126 au (Table S1), which are in between 0.1 and 0.2 au,[38] indicate that Fe−N bond is stronger than weak closed-shell interactions like ionic or van der Walls, and weaker than electron sharing (covalent) interactions. Complex **1** shows a slightly higher electron density $\rho(r)$ than that of complex **2** and is consistent with the Fe−$N_2$ bond lengths. Another factor that determines the type of interactions is the balanced ratio of positive kinetic electron energy density ($G(r)$) and negative potential electron energy density ($V(r)$), given as $-G(r)/V(r)$. A ratio greater than 1.0 indicates noncovalent interactions and that less than 0.5 indicates covalent interactions, and the value in between 0.5 and 1 represents a partial covalent character.[38] Complexes **1** and **2-quartet** show $-G(r)/V(r)$ ratios of 0.857 and 0.843 (Table S1), respectively, which demonstrate the partial covalent character of the Fe−$N_2$ bond. The negative total energy density values ($H(r)$) also support the partial covalent character of the Fe−$N_2$ bond. The ellipticity values are a measure of the bond order, and the ellipticity values of 0.06 and 0.11 of complexes **1** and **2-quartet** indicate a partial multiple bond character.

Table 2 provides the EDA-NOCV results of the Fe−N bond of complexes **1** and **2-quartet** calculated using dianionic $[(S)_2Fe]^{2-}$ in electronic triplet state and neutral $N_2$ fragment electronic singlet state as interacting fragments for complex **1**, and monoanionic $[(NacNac)(C_6H_5)Fe]^-$ in electronic quartet state, doublet state, and neutral $N_2$ fragment electronic singlet state as interacting fragments for **2-quartet** (Scheme 5). A careful examination of the molecular orbitals from NBO analysis helped in identifying the orbitals with unpaired electrons (Figures S2 and S3). The instantaneous interaction ($\Delta E_{int}$) indicates the intrinsic strength of the bond. Complexes **1** and **2-quartet** show almost similar instantaneous interaction (−76.7, −76.9 kcal mol$^{-1}$), albeit the slightly higher Pauli repulsion (8 kcal mol$^{-1}$) in **2-quartet**, while the intrinsic strength of complex **2-doublet** is further reduced, probably owing to higher Pauli repulsion. In addition, a higher electrostatic contribution (Table 2) arises from the difference in geometry. Note that the instantaneous interactions in **1** and **2-quartet** are reasonably higher than the bond dissociation energies, and the difference can be attributed to the preparative energy. The preparative energies originate from the mod-


https://doi.org/10.1021/acsomega.1c05238
ACS Omega 2021, 6, 33932−33942

**Table 2. EDA-NOCV Results at the BP86-D3(BJ)/TZ2P Level of Fe−$N_2$ Bonds of Complexes 1, 2-quartet, and 2-doublet Using Dianionic $[(S)_2Fe]^{2-}$ in Electronic Triplet State and Neutral $N_2$ Fragment Electronic Singlet State as Interacting Fragments for Complex 1 and Monoanionic $[(NacNac)(C_6H_5)Fe]^-$ in Electronic Quartet, Doublet States, and Neutral $N_2$ Fragment Electronic Singlet State as Interacting Fragments for Complex 2-quartet and 2-doublet, Respectively[a]**

| energy | interaction | $[(S)_2Fe]^{2-}$ (T) + $[N_2]$ (S) (1) | $[(NacNac)(C_6H_5)Fe]^-$ (Q) + $[N_2]$ (S) (2-quartet) | $[(NacNac)(C_6H_5)Fe]^-$ (D) + $[N_2]$ (S) (2-doublet) |
|---|---|---|---|---|
| $\Delta E_{int}$ | | −76.7 | −76.9 | −61.3 |
| $\Delta E_{Pauli}$ | | 158.3 | 165.3 | 181.8 |
| $\Delta E_{disp}$ [b] | | −6.4 (2.7%) | −4.5 (1.9%) | −5.3 (2.2%) |
| $\Delta E_{elstat}$ [b] | | −91.6 (39.0%) | −90.2 (37.2%) | −110.0 (45.2%) |
| $\Delta E_{orb}$ [b] | | −136.9 (58.3%) | −147.5 (60.9%) | −127.8 (52.6%) |
| $\Delta E_{orb(1)}$ [c] | (L)Fe → $N_2$ $\pi$ backdonation | −53.3 (38.9%) | −70.2 (47.6%) | −67.1 (52.5%) |
| $\Delta E_{orb(2)}$ [c] | (L)Fe → $N_2$ $\pi$ backdonation | −41.7 (30.5%) | −41.9 (28.4%) | −36.5 (28.6%) |
| $\Delta E_{orb(3)}$ [c] | (L)Fe ← $N_2$ $\sigma$ backdonation | −30.7 (22.4%) | −23.0 (15.6%) | −17.4 (13.6%) |
| $\Delta E_{orb(4)}$ [c] | (L)Fe ← $N_2$ $\sigma$ backdonation | | −7.1 (4.8%) | |
| $\Delta E_{orb(rest)}$ [c] | | −11.2 (8.2%) | −5.3 (3.6%) | −6.8 (5.3%) |

[a]Energies are in kcal $mol^{-1}$. [b]The values in the parentheses show the contribution to the total attractive interaction $\Delta E_{elstat} + \Delta E_{orb} + \Delta E_{disp}$. [c]The values in parentheses show the contribution to the total orbital interaction $\Delta E_{orb}$.

**Scheme 5. Schematic Representations of the Fragments with Corresponding Multiplicities Considered for the EDA-NOCV Calculation**

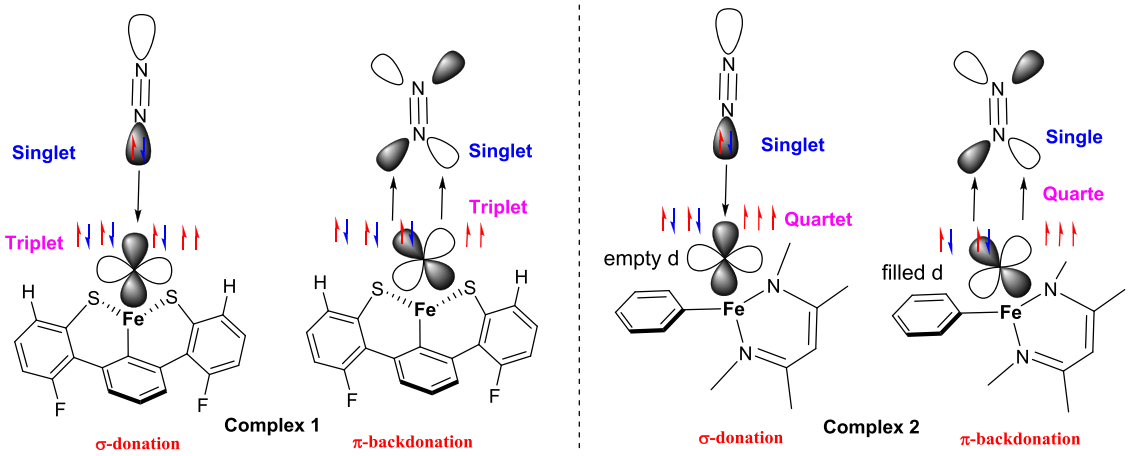


**Scheme 6. $\sigma$-Donation and $\pi$-Backdonation in Complexes 1 and 2-quartet[a]**

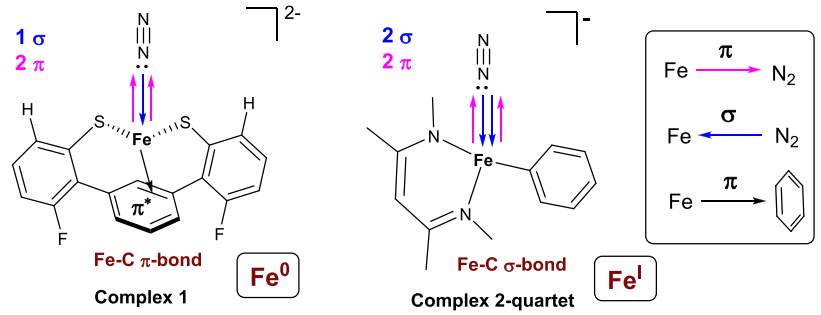


[a]See Figures 2 and 3 and Table 2 to obtain a quantitative idea about the strengths of each bonding interaction.

ifications in the geometry of the fragments from their equilibrium structure to the geometry in the compound, and also from the electronic excitation to a reference state.

The orbital (covalent) interactions are predominant and contribute 52.6−60.9% to the total attractive interactions in complexes **1**, **2-quartet** and **2-doublet**, while the electrostatic interactions contribute 37.2−45.2% and the dispersion contributes 1.9−2.7% to the total attractive interactions (Table 2). The higher orbital contributions indicate the covalent nature of the Fe−N bond. The pairwise interactions, resulting from the breakdown of the total orbital interactions, provide further insight into the type of interactions. Table 2 illustrates three pairwise contributions ($\Delta E_{orb(1-3)}$) for complex **1** and four pairwise contributions ($\Delta E_{orb(1-4)}$) for **2-quartet**. The largest orbital stabilization ($\Delta E_{orb(1)}$) comes from the Fe → $N_2$ $\pi$ electron backdonation followed by another Fe → $N_2$ $\pi$ backdonation ($\Delta E_{orb(2)}$) and Fe ← $N_2$ $\sigma$ electron donation ($\Delta E_{orb(3)}$) in complexes **1** and **2-quartet** (Scheme 6). Additionally, **2-quartet** shows another weak Fe ← $N_2$ $\sigma$ electron donation ($\Delta E_{orb(4)}$). The stronger Fe → $N_2$ $\pi$


https://doi.org/10.1021/acsomega.1c05238
ACS Omega 2021, 6, 33932−33942

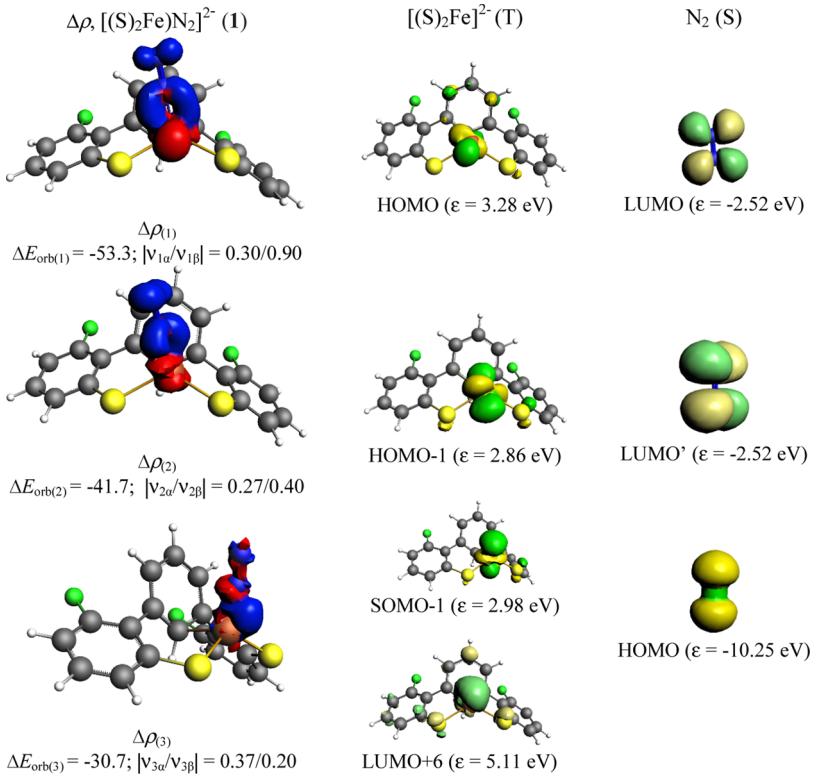


**Figure 2.** Shape of the deformation densities $\Delta\rho_{(1)-(3)}$ that correspond to $\Delta E_{orb(1)-(3)}$, and the associated MOs of $[(S)_2Fe)N_2]^{2-}$ (**1**) and the fragment orbitals of $[(S)_2Fe]^{2-}$ in triplet state and $N_2$ in the singlet state at the BP86-D3(BJ)/TZ2P level. Isosurface values of 0.003 au for $\Delta\rho_{(1-3)}$. The eigenvalues $|\nu_n|$ give the size of the charge migration in *e*. The direction of the charge flow of the deformation densities is red → blue.

backdonations contribute 69.4−76% to the orbital interactions in both complexes **1** and **2-quartet** and agree well with the charge distributions from the NBO analysis, whereas Fe ← $N_2$ $\sigma$ electron donations contribute 20.4−22.4% and equate well with the bonding analysis of M−N bonds in matrix isolated $M(N_2)_8$ (M = Ca, Sr, Ba) complexes, where M−N bonds are dominated by $M(d_\pi) \rightarrow (N_2)$ $\pi$ backdonations from metal orbitals.[37a,39]

The corresponding deformation densities $\Delta\rho_{(1-3/4)}$ associated with $\Delta E_{orb(1-3/4)}$ shown in Figures 2 2 and 3 reveal that the first Fe → $N_2$ $\pi$ backdonation $\Delta\rho_{(1)}$ is from HOMO (**1**) and HOMO−1 (**2-quartet**) ($d_{xy}$) orbitals of Fe into the vacant degenerate $\pi^*$ orbital LUMO ($1\pi_g$) of $N_2$, whereas the second Fe → $N_2$ $\pi$ backdonation $\Delta\rho_{(2)}$ is from HOMO−1 (**1**) and HOMO (**2-quartet**) ($d_{yz}$) orbitals of Fe into the vacant degenerate $\pi^*$ orbital LUMO′ ($1\pi_g'$) of $N_2$ (Scheme 5). The third deformation density $\Delta\rho_{(3)}$ represents the Fe ← $N_2$ $\sigma$ electron donation from HOMO ($3\sigma_g^+$; filled bonding $\sigma_{2s}^*$ with the same phase (+, +)) of $N_2$, along with the slight polarization (hybridization) within the fragment from $d_{z^2}$ orbital (SOMO−1/SOMO−2) of Fe into the vacant LUMO+6 and LUMO+1 orbitals of Fe in complexes **1** and **2-quartet**, respectively. Besides the three major deformation densities, complex **2-quartet** shows another weak deformation density $\Delta\rho_{(4)}$, which is similar in shape to $\Delta\rho_{(3)}$, but the electron donation is from HOMO−2 ($2\sigma_u^+$; filled antibonding $\sigma_{2s}^*$ with opposite phase (+, −)) of $N_2$ (Figure 3; Scheme 1, top), which might have led to deviation of the Fe−N−N angle (174°) from 180°. Complex **2-doublet** shows three pairwise contributions, which reveal stronger Fe → $N_2$ $\pi$ backdonations and slightly weaker Fe ← $N_2$ $\sigma$ donation (Table 2) compared to that of the complex **2-quartet**. The deformation densities of the complex **2-doublet** can be seen in Figure S5.

The aromaticity of the benzene/phenyl ring in complexes **1** and **2-quartet**, their precursor complexes, and ligands has been measured by calculating the magnetic NICS, introduced by Schleyer et al.,[40] using the gauge-independent atomic orbital (GIAO) approach at BP86/def2-TZVPP level on the geometries optimized at BP86-D3(BJ)/def2-TZVPP level. The NICS method is considered as a popular probe of aromaticity due to its ability to describe the aromaticity, antiaromaticity, and non-aromaticity of ring systems both qualitatively and quantitatively.[41] The NICS values calculated at the geometric centers of the ring are termed as NICS(0) and is considered as a measure of the $\sigma + \pi$ electron delocalization, whereas the values calculated at 1 Å above the plane of the ring are designated as NICS(1), which represents $\pi$-electron delocalization.[42]

Negative NICS values specify aromaticity and positive NICS values indicate antiaromaticity, while values close to zero represent non-aromaticity. A close inspection of the NICS values from Table 3 shows that the aromaticity of the dithiolate $(S_2)^-$ ligand decreases on coordinating to iron and then again increases upon interacting with $N_2$ in complex **1**. The reduction in the aromaticity on coordinating to metal is comparable to that of metallabenzynes.[43]

On similar lines, the precursor of complex **2-quartet** shows an increase in aromaticity after binding to $N_2$. The decrease in the aromaticity of the fragments $[S_2Fe]^-$ and $[(NacNac)\text{-}C_6H_5)Fe]^-$ (Table 3) can be attributed to the backdonation from Fe into the $\pi^*$ orbital of the aromatic carbon as expected. Olefins are often seen to form a $\pi$-complex with the transition metals. The donor−acceptor type bonds between metal-atom


https://doi.org/10.1021/acsomega.1c05238
ACS Omega 2021, 6, 33932−33942

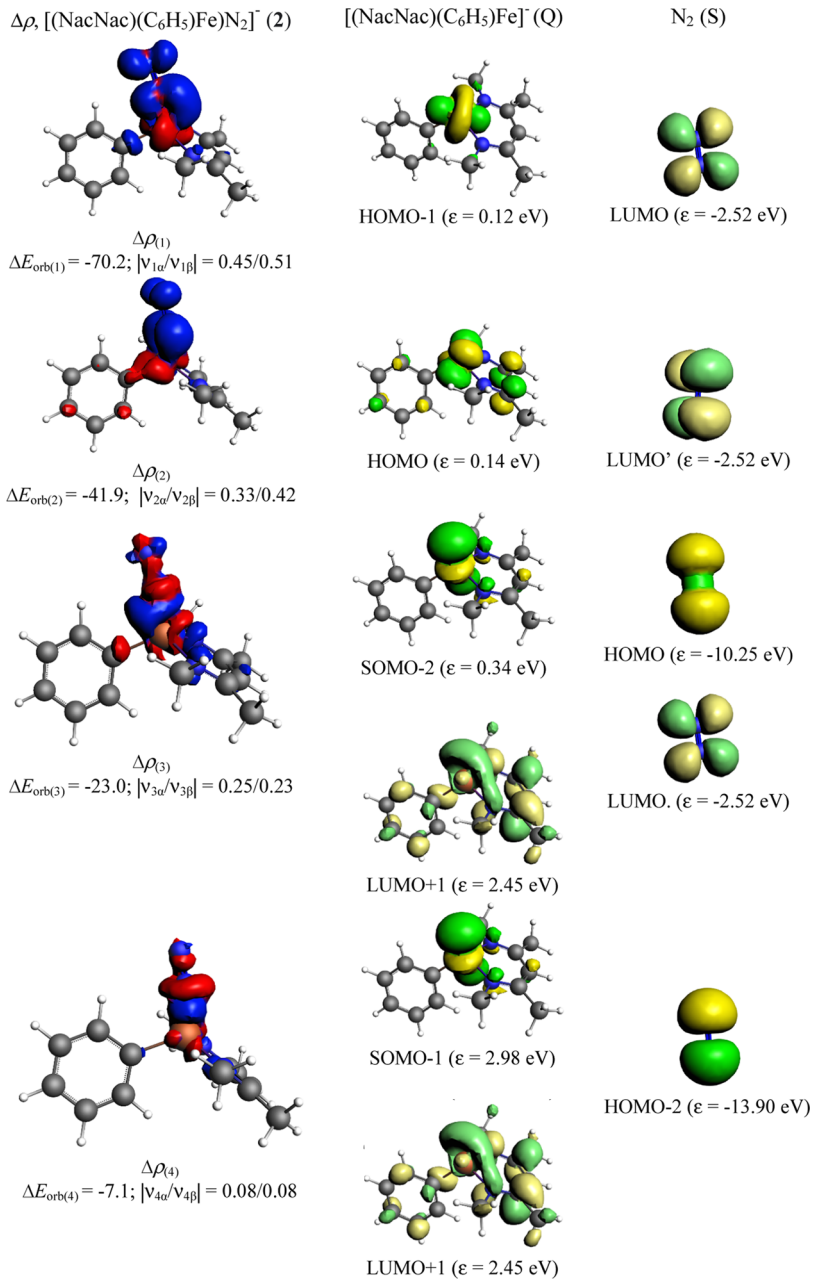


**Figure 3.** Shape of the deformation densities $\Delta\rho_{(1)-(4)}$ that correspond to $\Delta E_{orb(1)-(4)}$, and the associated MOs of $[(NacNac)(C_6H_5)Fe)N_2]^-$ (**2-quartet**) and the fragment orbitals of $[(NacNac)(C_6H_5)Fe]^-$ in quartet state and $N_2$ in the singlet state at the BP86-D3(BJ)/TZ2P level. Isosurface values of 0.003 au for $\Delta\rho_{(1-4)}$. The eigenvalues $|\nu_n|$ give the size of the charge migration in *e*. The direction of the charge flow of the deformation densities is red → blue.

**Table 3. NICS(0/1) Results of 1, 2-quartet, and 2-doublet and Their Precursors at the BP86/Def2TZVPP Level**

| compound | NICS(0) | NICS(1) |
|---|---|---|
| $S_2$ ligand | −6.49 | −7.92 |
| $[S_2Fe]^{2-}$ | −2.29 | −1.72 |
| complex **1** | −8.03 | −5.89 |
| $[(NacNac)C_6H_5)Fe]^-$ | −4.79 | −7.98 |
| complex **2-quartet** | −5.47 | −8.63 |
| complex **2-doublet** | −5.02 | −8.03 |

and olefins are speculated. However, after binding to $N_2$ the Fe → $N_2$ $\pi$-backdonation increases, which eventually changes the direction of charge flow from C → Fe → $N_2$ as shown by NBO calculations. Additionally, the slight increase in Fe−C bond length (0.06 Å) after binding to $N_2$ supports the change in the direction of charge flow. This triggers the increase in aromaticity in complexes **1** and **2-quartet** as shown in Table 3. Scheme 7 shows the location of NICS(0) and NICS(1) in the molecules represented in Table 3. The NBO pictures (Figure 4) of **1** and **2-quartet** (right) showed the orbital interactions between the d-orbitals of Fe atoms and the $\pi$-orbital of benzene/phenyl ring (double-headed arrow). It is known that aromatic rings will possess a diamagnetic ring current, while the antiaromatic and paramagnetic species will induce a paramagnetic ring current under applied magnetic field. The true picture of the aromaticity of the benzene/phenyl ring of these two complexes could be even more


https://doi.org/10.1021/acsomega.1c05238
ACS Omega 2021, 6, 33932−33942

**Scheme 7. Schematic Representation of NICS(0) and NICS(1) in the Molecules Represented in Table 3**[a]

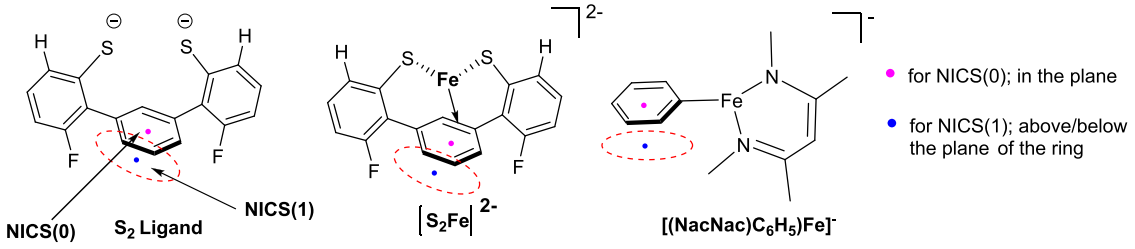


[a]Pink point for NICS(0): a point in the plane of the $C_6$ ring. Blue point for NICS(1): a point in the plane above/below the plane of the ring.

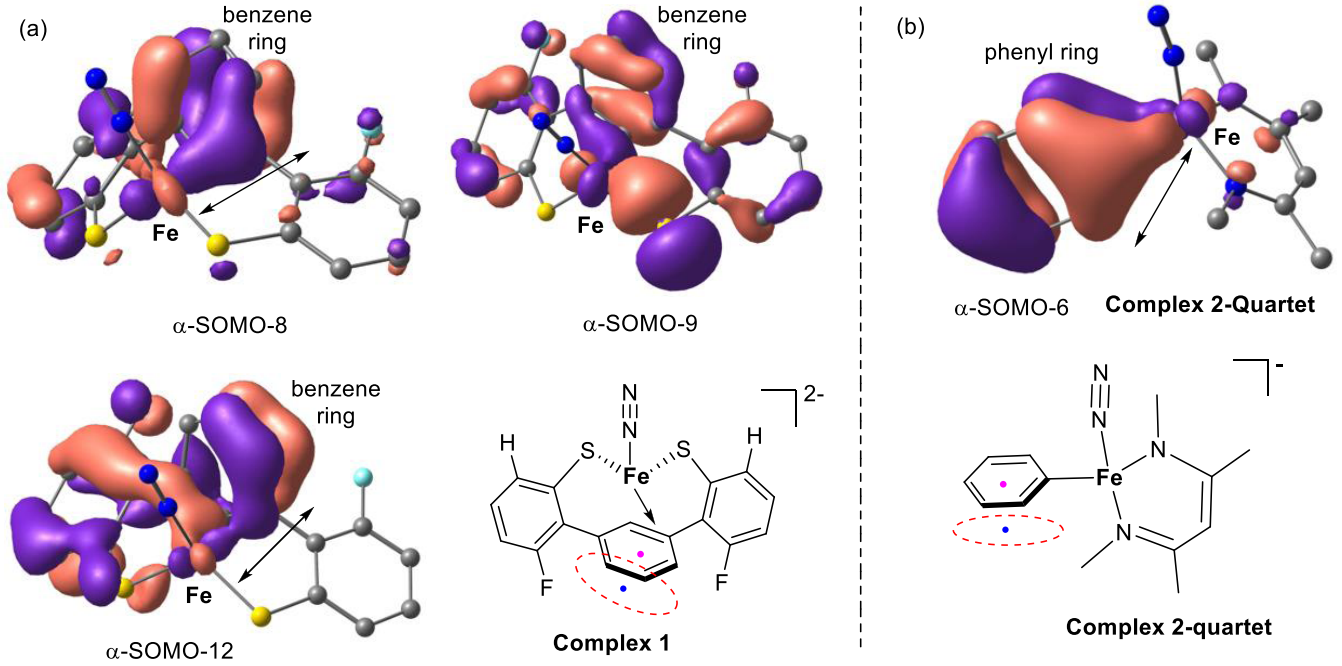


**Figure 4.** NBOs of complex **1** (left) and **2-quartet** (right) showing the orbital interactions between Fe and the $\pi$-orbital of the benzene/phenyl ring (double-headed arrow).

complex than it appears. The bottom point is that Fe-aromatic-ring interactions are somehow related to the $N_2$ ($\pi$-accepting ligand) binding similar to the (benzene)−$M(CO)_{n-1}$−CO.

## SUMMARY AND CONCLUSION

In conclusion, we have reported the EDA-NOCV and NICS analyses of dithiolate-$Fe^0$-$N_2$ (**1**) and L-$Fe^I(N_2)$(Ph) (**2**), which can be regarded as model complexes with relevance to the nitrogen-fixing FeMoco cofactor of the nitrogenase enzyme. The quantum mechanical calculations on **2** with smaller substitutions suggest that **B** (with bulkier substituents on N atoms of L) is more likely to have a quartet ground state than a doublet state. The calculations suggested the endothermic dissociation of Fe−$N_2$ bond [$(L)Fe^{0/I}-N_2 \rightarrow (L)Fe^{0/I} + N_2$] in complexes **1**−**2**. NBO calculations indicate the direction of charge flow from metal to dinitrogen [(L) → Fe → $N_2$], which rationalizes the activation N≡N bond. The EDA-NOCV analysis shows higher orbital contributions, indicating a higher covalent character than the ionic character of the Fe−$N_2$ bond. The pairwise orbital interactions suggest that the combination of two $\pi$-backdonations [$(d)_{Fe} \rightarrow (\pi^*)_{N2}$] is much stronger than $\sigma$-donation [$(\sigma_{1s/2s})_{N2} \rightarrow (d)_{Fe}$], which has been schematically represented in Schemes 5 and 6 and pictorially/quantitatively displayed in Figures 2 and 3/Table 2. The $\Delta E_{int}$ values of the Fe−$N_2$ bonds of these two complexes are in the range of 76−77 kcal $mol^{-1}$. Additionally, NICS calculations suggest that the Fe(0/I) → C($\pi^*$; aromatic ring) $\pi$-backdonations are significantly stronger before $N_2$ binding (Table 3). The computed $\sigma$- and $\pi$-aromaticities corresponding to **1**−**2-quartet** are significantly lower after dinitrogen binding due to the flow of electron densities from the Fe centers to $N_2$. However, the complexes **1** and **2-quartet** differ in the magnitude of $\sigma$- and $\pi$-aromaticities due to the difference in the position of the Fe atom and also oxidation state.

## ASSOCIATED CONTENT

### Supporting Information

The Supporting Information is available free of charge at https://pubs.acs.org/doi/10.1021/acsomega.1c05238.

Computational methods, tables, figures, QTAIM and optimized coordinates (PDF)

## AUTHOR INFORMATION

### Corresponding Author

**Kartik Chandra Mondal** − *Department of Chemistry, Indian Institute of Technology Madras, Chennai 600036, India;*



https://doi.org/10.1021/acsomega.1c05238
ACS Omega 2021, 6, 33932−33942

orcid.org/0000-0002-5830-3608; Email: csdkartik@iitm.ac.in

### Author

**Sai Manoj N. V. T. Gorantla** − *Department of Chemistry, Indian Institute of Technology Madras, Chennai 600036, India;* orcid.org/0000-0001-7315-6354

Complete contact information is available at: https://pubs.acs.org/10.1021/acsomega.1c05238

### Notes

The authors declare no competing financial interest.

## ■ ACKNOWLEDGMENTS

The authors thank Prof. Gernot Frenking and Prof. K.M.S. for providing computational facilities. S.M.N.V.T.G. also thanks Dr. S. Pan for valuable suggestions. S.M.N.V.T.G. thanks CSIR for SRF. K.C.M. thanks SERB for the ECR grant (ECR/2016/000890) and IIT Madras for the seed grant.

## ■ REFERENCES

(1) Hoffman, B. M.; Dean, D. R.; Seefeldt, L. C. Climbing Nitrogenase: Toward a Mechanism of Enzymatic Nitrogen Fixation. *Acc. Chem. Res.* **2009**, *42*, 609.
(2) Crossland, J. L.; Tyler, D. R. Iron−dinitrogen coordination chemistry: Dinitrogen activation and reactivity. *Coord. Chem. Rev.* **2010**, *254*, 1883.
(3) Rittle, J.; Peters, J. C. Fe−$N_2$/CO complexes that model a possible role for the interstitial C atom of FeMo-cofactor (FeMoco). *Proc. Natl. Acad. Sci. U.S.A.* **2013**, *110*, 15898.
(4) Minteer, S. D.; Christopher, P.; Linic, S. Recent Developments in Nitrogen Reduction Catalysts: A Virtual Issue. *ACS Energy Lett.* **2019**, *4*, 163−166.
(5) Zhao, L.; Pan, S.; Holzmann, N.; Schwerdtfeger, P.; Frenking, G. Chemical Bonding and Bonding Models of Main-Group Compounds. *Chem. Rev.* **2019**, *119*, 8781.
(6) Cai, R.; Minteer, S. D. Nitrogenase Bioelectrocatalysis: From Understanding Electron-Transfer Mechanisms to Energy Applications. *ACS Energy Lett.* **2018**, *3*, 2736.
(7) Bjornsson, R.; Neese, F.; DeBeer, S. Revisiting the Mössbauer Isomer Shifts of the FeMoco Cluster of Nitrogenase and the Cofactor Charge. *Inorg. Chem.* **2017**, *56*, 1470.
(8) Matson, B. D.; Peters, J. C. Fe-Mediated HER vs $N_2$RR: Exploring Factors That Contribute to Selectivity in $P_3^EFe(N_2)$ (E = B, Si, C) Catalyst Model Systems. *ACS Catal.* **2018**, *8*, 1448.
(9) Lee, Y.; Sloane, F. T.; Blondin, G.; Abboud, K. A.; García-Serres, R.; Murray, L. J. Dinitrogen Activation upon Reduction of a Triiron(II) Complex. *Angew. Chem., Int. Ed.* **2015**, *54*, 1499.
(10) Ćorić, I.; Holland, P. L. Insight into the Iron−Molybdenum Cofactor of Nitrogenase from Synthetic Iron Complexes with Sulfur, Carbon, and Hydride Ligands. *J. Am. Chem. Soc.* **2016**, *138*, 7200.
(11) Wickramasinghe, L. A.; Ogawa, T.; Schrock, R. R.; Müller, P. Reduction of Dinitrogen to Ammonia Catalyzed by Molybdenum Diamido Complexes. *J. Am. Chem. Soc.* **2017**, *139*, 9132.
(12) Fajardo, J., Jr.; Peters, J. C. Catalytic Nitrogen-to-Ammonia Conversion by Osmium and Ruthenium Complexes. *J. Am. Chem. Soc.* **2017**, *139*, 16105.
(13) Lindley, B. M.; van Alten, R. S.; Finger, M.; Schendzielorz, F.; Würtele, C.; Miller, A. J. M.; Siewert, I.; Schneider, S. Mechanism of Chemical and Electrochemical $N_2$ Splitting by a Rhenium Pincer Complex. *J. Am. Chem. Soc.* **2018**, *140*, 7922.
(14) Sekiguchi, Y.; Arashiba, K.; Tanaka, H.; Eizawa, A.; Nakajima, K.; Yoshizawa, K.; Nishibayashi, Y. Catalytic Reduction of Molecular Dinitrogen to Ammonia and Hydrazine Using Vanadium Complexes. *Angew. Chem., Int. Ed.* **2018**, *57*, 9064.
(15) Yao, Y.; Zhu, S.; Wang, H.; Li, H.; Shao, M. A Spectroscopic Study on the Nitrogen Electrochemical Reduction Reaction on Gold and Platinum Surfaces. *J. Am. Chem. Soc.* **2018**, *140*, 1496.
(16) Rittle, J.; Peters, J. C. Fe−$N_2$/CO complexes that model a possible role for the interstitial C atom of FeMo-cofactor (FeMoco). *Proc. Natl. Acad. Sci. U.S.A.* **2013**, *110*, 15898.
(17) Bruch, Q. J.; Connor, G. P.; McMillion, N. D.; Goldman, A. S.; Hasanayn, F.; Holland, P. L.; Miller, A. J. M. Considering Electrocatalytic Ammonia Synthesis via Bimetallic Dinitrogen Cleavage. *ACS Catal.* **2020**, *10*, 10826.
(18) Ung, G.; Peters, J. C. Low-Temperature $N_2$ Binding to Two-Coordinate $L_2Fe^0$ Enables Reductive Trapping of $L_2FeN_2^-$ and $NH_3$ Generation. *Angew. Chem., Int. Ed.* **2015**, *54*, 532.
(19) Mankad, N. P.; Whited, M. T.; Peters, J. C. Terminal $Fe^I$−$N_2$ and $Fe^{II}$···H−C Interactions Supported by Tris(phosphino)silyl Ligands. *Angew. Chem., Int. Ed.* **2007**, *46*, 5768.
(20) Lee, Y.; Mankad, N. P.; Peters, J. C. Triggering $N_2$ uptake via redox-induced expulsion of coordinated $NH_3$ and $N_2$ silylation at trigonal bipyramidal iron. *Nat. Chem.* **2010**, *2*, 558.
(21) Creutz, S. E.; Peters, J. C. Catalytic Reduction of $N_2$ to $NH_3$ by an Fe−$N_2$ Complex Featuring a C-Atom Anchor. *J. Am. Chem. Soc.* **2014**, *136*, 1105.
(22) Hill, P. J.; Doyle, L. R.; Crawford, A. D.; Myers, W. K.; Ashley, A. E. Selective Catalytic Reduction of $N_2$ to $N_2H_4$ by a Simple Fe Complex. *J. Am. Chem. Soc.* **2016**, *138*, 13521.
(23) Bazhenova, T. A.; Shilov, A. E. Nitrogen fixation in solution. *Coord. Chem. Rev.* **1995**, *144*, 69.
(24) Kuriyama, S.; Arashiba, K.; Nakajima, K.; Matsuo, Y.; Tanaka, H.; Ishii, K.; Yoshizawa, K.; Nishibayashi, Y. Catalytic transformation of dinitrogen into ammonia and hydrazine by iron-dinitrogen complexes bearing pincer ligand. *Nat. Commun.* **2016**, *7*, No. 12181.
(25) Thompson, N. B.; Green, M. T.; Peters, J. C. Nitrogen Fixation via a Terminal Fe(IV) Nitride. *J. Am. Chem. Soc.* **2017**, *139*, 15312.
(26) Ćorić, I.; Mercado, B. Q.; Bill, E.; Vinyard, D. J.; Holland, P. L. Binding of Dinitrogen to an Iron-Sulfur-Carbon Site. *Nature* **2015**, *526*, 96.
(27) McWilliams, S. F.; Broere, D. L. J.; Halliday, C. J. V.; Bhutto, S. M.; Mercado, B. Q.; Holland, P. L. Coupling dinitrogen and hydrocarbons through aryl migration. *Nature* **2020**, *584*, 221.
(28) Mitoraj, M.; Michalak, A. Donor−Acceptor Properties of Ligands from the Natural Orbitals for Chemical Valence. *Organometallics* **2007**, *26*, 6576.
(29) Mitoraj, M.; Michalak, A. Applications of natural orbitals for chemical valence in a description of bonding in conjugated molecules. *J. Mol. Model.* **2008**, *14*, 681.
(30) ADF2017. *SCM, Theoretical Chemistry*; Vrije Universiteit: Amsterdam, The Netherlands, 2021. http://www.scm.com (accessed Jan 9, 2021).
(31) te Velde, G.; Bickelhaupt, F. M.; Baerends, E. J.; Guerra, C. F.; van Gisbergen, S. J. A.; Snijders, J. G.; Ziegler, T. Chemistry with ADF. *J. Comput. Chem.* **2001**, *22*, 931.
(32) van Lenthe, E.; Baerends, E. J. Optimized Slater-type basis sets for the elements 1−118. *J. Comput. Chem.* **2003**, *24*, 1142.
(33) van Lenthe, E.; Baerends, E. J.; Snijders, J. G. Relativistic regular two-component Hamiltonians. *J. Chem. Phys.* **1993**, *99*, 4597.
(34) van Lenthe, E.; Baerends, E. J.; Snijders, J. G. Relativistic total energy using regular approximations. *J. Chem. Phys.* **1994**, *101*, 9783.
(35) (a) Frenking, G.; Bickelhaupt, F. M. The EDA Perspective of Chemical Bonding. In *The Chemical Bond 1. Fundamental Aspects of Chemical Bonding*; Wiley-VCH: Weinheim, 2014; p 121. (b) Zhao, L. M.; von Hopffgarten; Andrada, D. M.; Frenking, G. Energy decomposition analysis. *WIREs Comput. Mol. Sci.* **2018**, *8*, 1345. (c) Zhao, L.; Hermann, M.; Schwarz, W. H. E.; Frenking, G. The Lewis electron-pair bonding model: modern energy decomposition analysis. *Nat. Rev. Chem.* **2019**, *3*, 48. (d) Yang, W.; Krantz, K. E.; Freeman, L. A.; Dickie, D.; Molino, A.; Frenking, G.; Pan, S.; Wilson, D. J. D.; Gilliard Jr, R. J. Persistent Borafluorene Radicals. *Angew. Chem., Int. Ed.* **2020**, *59*, 3850.

(36) Andrés, J.; Ayers, P. W.; Boto, R. A.; Carbó-Dorca, R.; Chermette, H.; Cioslowski, J.; Contreras-García, J.; Cooper, D. L.; Frenking, G.; Gatti, C.; Heidar-Zadeh, F.; Joubert, L.; Martín Pendás, A.; Matito, E.; Mayer, I.; Misquitta, A. J.; Mo, Y.; Pilmé, J.; Popelier, P. L. A.; Rahm, M.; Ramos-Cordoba, E.; Salvador, P.; Schwarz, W. H. E.; Shahbazian, S.; Silvi, B.; Solà, M.; Szalewicz, K.; Tognetti, V.; Weinhold, F.; Zins, E. L. Nine questions on energy decomposition analysis. *J. Comput. Chem.* **2019**, *40*, 2248.

(37) (a) Wang, Q.; Pan, S.; Lei, S.; Jin, J.; Deng, G.; Wang, G.; Zhao, L.; Zhou, M.; Frenking, G. Octa-Coordinated Alkaline Earth Metal−Dinitrogen Complexes $M(N_2)_8$ (M = Ca, Sr, Ba). *Nat. Commun.* **2019**, *10*, No. 3375. (b) Bondì, L.; Garden, A. L.; Jerabek, P.; Totti, F.; Brooker, S. Quantitative and Chemically Intuitive Evaluation of the Nature of M−L Bonds in Paramagnetic Compounds: Application of EDA-NOCV Theory to Spin Crossover Complexes. *Chem. - Eur. J.* **2020**, *26*, 13677. (c) Kneusels, N. J. H.; Münzer, J. E.; Flosdorf, K.; Jiang, D.; Neumüller, B.; Zhao, L.; Eichhöfer, A.; Frenking, G.; Kuzu, I. Double Donation in Trigonal Planar Iron-Carbodiphosphorane Complexes-a Concise Study on Their Spectroscopic and Electronic Properties. *Dalton Trans.* **2020**, *49*, 2537.

(38) (a) Matta, C. F.; Boyd, R. J. Chapter 1. An Introduction to the Quantum Theory of Atoms in Molecules. In *The Quantum Theory of Atoms in Molecules: From Solid State to DNA and Drug Design*; Wiley: Hoboken, 2007; pp 1−34. (b) Bader, R. F. W. Atoms in molecules. *Acc. Chem. Res.* **1985**, *18*, 9. (c) Bader, R. F. W. A quantum theory of molecular structure and its applications. *Chem. Rev.* **1991**, *91*, 893−928. (d) Kumar, P. S. V.; Raghavendra, V.; Subramanian, V. Bader's Theory of Atoms in Molecules (AIM) and its Applications to Chemical Bonding. *J. Chem. Sci.* **2016**, *128*, 1527.

(39) Rösch, B.; Gentner, T. X.; Langer, J.; Färber, C.; Eyselein, J.; Zhao, L.; Ding, C.; Frenking, G.; Harder, S. Dinitrogen complexation and reduction at low-valent calcium. *Science* **2021**, *371*, 1125.

(40) Chen, Z.; Wannere, C. S.; Corminboeuf, C.; Puchta, R.; Schleyer, P. vR. Nucleus-Independent Chemical Shifts (NICS) as an Aromaticity Criterion. *Chem. Rev.* **2005**, *105*, 3842.

(41) Feixas, F.; Matito, E.; Poater, J.; Solà, M. Quantifying Aromaticity with Electron Delocalisation Measures. *Chem. Soc. Rev.* **2015**, *44*, 6434.

(42) Baryshnikov, G. V.; Minaev, B. F.; Pittelkow, M.; Nielsen, C. B.; Salcedo, R. Nucleus-independent chemical shift criterion for aromaticity in π-extended tetraoxa[8]circulenes. *J. Mol. Model.* **2013**, *19*, 847−850.

(43) Fernández, I.; Frenking, G.; Merino, G. Aromaticity of Metallabenzenes and Related Compounds. *Chem. Soc. Rev.* **2015**, *44*, 6452.



https://doi.org/10.1021/acsomega.1c05238
*ACS Omega* 2021, 6, 33932−33942